Eur. Phys. J. C (2018) 78:49
https://doi.org/10.1140/epjc/s10052-018-5515-8

THE EUROPEAN PHYSICAL JOURNAL C

Regular Article - Theoretical Physics

Holographic Van der Waals phase transition of the higher-dimensional electrically charged hairy black hole

Hui-Ling Li[1,2,a], **Zhong-Wen Feng**[3], **Xiao-Tao Zu**[1]

[1] School of Physical Electronics, University of Electronic Science and Technology of China, Chengdu 610054, China
[2] College of Physics Science and Technology, Shenyang Normal University, Shenyang 110034, China
[3] College of Physics and Space Science, China West Normal University, Nanchong 637002, China

Received: 7 May 2017 / Accepted: 30 December 2017 / Published online: 20 January 2018

Abstract With motivation by holography, employing black hole entropy, two-point connection function and entanglement entropy, we show that, for the higher-dimensional Anti-de Sitter charged hairy black hole in the fixed charged ensemble, a Van der Waals-like phase transition can be observed. Furthermore, based on the Maxwell equal-area construction, we check numerically the equal-area law for a first order phase transition in order to further characterize the Van der Waals-like phase transition.

1 Introduction

According to the Anti-de Sitter space/Conformal Field Theory (AdS/CFT) correspondence [1], the thermodynamics of AdS black holes plays a key role in comprehending the thermal properties of the holographically dual field theories. To the compelling phenomena of thermodynamics belong phase transitions in AdS spacetime. The pioneer discussion of phase transitions was presented by Hawking and Page [2]. In 1983, in a four-dimensional non-charged AdS background, Hawking and Page proved that there exists a first order phase transition between the AdS and Schwarzschild AdS black hole. Specifically speaking, the thermal AdS is unstable, and it has to undergo a phase transition to the stable Schwarzschild AdS black hole at last, which is the best-known Hawking–Page phase transition.

Later, in 1999, in a charged AdS background, Chamblin et al. [3,4] explored the phase structure of an Reissner–Nordström AdS black hole. Compared to the non-charged AdS case, the charged black hole's phase structure becomes richer and is associated with the chosen statistical ensemble. It was found that the charged AdS black hole in the temperature–entropy plane presented an analogous Van der Waals phase transition in the canonical ensemble (fixed electric charge), i.e. the isocharge in the temperature–entropy plane has an unstable branch and two stable ones when the charge below a critical value. And there exists a second order critical point at a critical charge. Recently, the research on a Van der Waals-like phase transition has been generalized to the extended phase space [5–10]. In this framework, the cosmological constant is taken as a thermodynamical pressure, and its conjugate quantity is treated as the thermodynamical volume. Consequently, this extended phase space makes the Van de Waals description more precise.

Very recently, entanglement entropy has also been used to detect phase structures in different AdS backgrounds. Johnson [11] proposed that, like black hole entropy, entanglement entropy also exhibited a Van der Waals-like phase transition in the temperature-entanglement entropy plane in both the fixed potential ensemble and the charge ensemble. It was subsequently generalized to supergravity STU black holes that involve four charges by Caceres et al. [12]. The result showed that Van der Waals behavior was observed in the cases of three charge and four charge, however, for the one-charge and two-charge cases, the STU black holes did not present this phase transition. Caceres et al. also verified that, for a charge configuration that presented a Van der Waals-like phase transition, the entanglement entropy indeed exhibits a similar phase transition at the same critical temperature and the same critical exponents as the ones obtained in the black hole entropy. Furthermore, the equal-area law of entanglement entropy was also checked by Nguyen [13] for an AdS Reissner–Nordström black hole in the canonical ensemble. In addition, Zeng et al. have investigated phase structures of holographic entanglement entropy in massive gravity [14], in the Born–Infeld Anti-de Sitter background [15] and in the quintessence Reissner–Nordström AdS background [16], and all the results showed that there exists a Van de Waals-like phase transition in these gravity backgrounds [14–18].

[a] e-mail: LHL51759@126.com

In the framework of holography, in higher-dimensional AdS spacetime, it is interesting to detect the phase structure of hairy black holes. Since there exist hair parameters, hairy black hole solutions become far richer than in General Relativity [19,20]. The model for higher-dimensional hairy black holes was first introduced by Oliva and Ray in 2011. They developed a novel construction of conformal couplings of a scalar field to arbitrary higher order Euler densities, and further solved the equations of motion under spherically symmetric conditions [21]. Although hairy black holes with vanishing cosmological constant are known in four dimensions, the scalar field configuration of these black holes diverges at the horizon [22,23]. This may be seen as a natural consequence of the well-known no-hair theorems. However, by introducing a cosmological constant and a conformal coupling, no-hair theorems can be circumvented. In 2014, in higher-dimensional AdS spacetime, Giribet et al. proved that analytic solutions to higher-dimensional hairy black holes do exist and the scalar configuration is regular everywhere outside and on the horizon. It turned out that the hairy solution asymptotically goes to (Anti-) de Sitter spacetime at large distance and admits a spherical horizon as well as a horizon of a different topology [24]. In 2015, the thermodynamics of higher-dimensional hairy black holes and the different phases of hairy black holes in AdS5 space were also studied in detail [25,26]. At the same time, for these hairy solutions in a five-dimensional gravitational system, Hennigar and Mann have first revealed a reentrant phase transition in the case of demanding the positivity of entropy [7]. In 2017, Hennigar, Mann and Tjoa have found that, for a class of asymptotically AdS hairy black holes in Lovelock gravity where a real scalar field is conformally coupled to gravity, a novel form of phase transition akin to a superfluid phase transition can be observed [27]. Here, employing the black hole entropy, two-point correlated function and entanglement entropy, we attempt to study whether the Van der Waals-like phase transition can be observed, and we discuss the hair parameter effect on the phase transition.

2 Phase transition and Maxwell's equal-area law for the thermodynamic entropy

Let us start by reviewing the exact solution of an electrically charged hairy black hole in five dimensions. Einstein–Maxwell-Λ theory conformally coupled to a scalar field in higher dimensions and see whether it can exhibit analytic solutions [24,25]. Here, we are concerned with the case of five dimensions, and the action of the theory reads

$$I=\frac{1}{\kappa}\int \mathrm{d}^5x\sqrt{-g}\left[R-2\Lambda-\frac{1}{4}F^2+\kappa L_m\left(\phi,\nabla\phi\right)\right], \tag{1}$$

where

$$\kappa=16\pi G, \tag{2}$$

$$L_m\left(\phi,\nabla\phi\right)=b_0\phi^{15}+b_1\phi^7 S_{\mu\nu}{}^{\mu\nu}+b_2\phi^{-1}\big(S_{\mu\gamma}{}^{\mu\gamma}S_{\nu\delta}{}^{\nu\delta}-4S_{\mu\gamma}{}^{\nu\gamma}S_{\nu\delta}{}^{\mu\delta}+S_{\mu\nu}{}^{\gamma\delta}S^{\nu\mu}{}_{\gamma\delta}\big), \tag{3}$$

$$S_{\mu\nu}{}^{\gamma\delta}=\phi^2R_{\mu\nu}{}^{\gamma\delta}-12\delta^{[\gamma}_{[\mu}\delta^{\delta]}_{\nu]}\nabla_\rho\phi\nabla^\rho\phi-48\phi\delta^{[\gamma}_{[\mu}\nabla_{\nu]}\nabla^{\delta]}\phi+18\delta^{[\gamma}_{[\mu}\nabla_{\nu]}\phi\nabla^{\delta]}\phi. \tag{4}$$

Here, b_0, b_1 and b_2 are real coupling constants, which are generated by a real scalar the field conformally coupled to gravity. The static spherically symmetric black hole solution coming from the action (1) can be written as

$$\mathrm{d}s^2=-N^2\left(r\right)f\left(r\right)\mathrm{d}t^2+\frac{\mathrm{d}r^2}{g\left(r\right)}+r^2\mathrm{d}\Omega_3^2, \tag{5}$$

where

$$g\left(r\right)=f\left(r\right)=1-\frac{m}{r^2}-\frac{q}{r^3}+\frac{e^2}{r^4}+\frac{r^2}{l^2},\quad N^2\left(r\right)=1. \tag{6}$$

Here, l is AdS radius $l^2=-6/\Lambda$, and $\mathrm{d}\Omega_3^2$ is the metric of the unit 3-sphere. The integration constants m and e are related with the mass and the electric charge of the hairy black hole, and q is given with respect to the scalar coupling constants by the relation

$$q=\frac{64\pi G}{5}\varepsilon b_1\left(-\frac{18b_1}{5b_0}\right)^{3/2}, \tag{7}$$

where $\varepsilon=-1,\ 0,\ +1$. For the five-dimensional black hole solution to exist, the scalar coupling constants must obey the following constraint:

$$10b_0b_2=9b_1^2. \tag{8}$$

The Maxwell potential is

$$A_\mu=\sqrt{3}\frac{e}{r^2}\delta^0_\mu \tag{9}$$

with $F_{\mu\nu}=\partial_\mu A_\nu-\partial_\nu A_\mu$. On the other hand, the scalar field configuration takes the form

$$\phi\left(r\right)=\frac{n}{r^{1/3}},\qquad n=\varepsilon\left(-\frac{18}{5}\frac{b_1}{b_0}\right)^{1/6}. \tag{10}$$

In Ref. [25], Galante et al. have discussed the thermodynamic properties of higher-dimensional black holes in detail. The mass and charge of the hairy black hole are

$$M=\frac{3\pi}{8}m=\frac{3\pi\left(e^2l^2-ql^2r_+ +l^2r_+^4-r_+^6\right)}{8l^2r_+^2} \tag{11}$$

and

$$Q=-\frac{\sqrt{3}\pi}{8}e, \tag{12}$$

respectively, where r_+ is the event horizon, which is given by the equation $f(r_+) = 0$. The Hawking temperature and black hole entropy are given by [7,25]

$$T = \frac{1}{\pi l^2 r_+^4}\left(-\frac{32Q^2l^2}{3\pi^2 r_+} + \frac{ql^2}{4} + \frac{l^2}{2}r_+^3 + r_+^5\right), \tag{13}$$

$$S = \frac{\pi^2}{2}\left(r_+^3 - \frac{5}{2}q\right). \tag{14}$$

Note that, for the hairy black hole solution to exist, q can take three different values namely $q = 0, \pm|q|$. For $q = 0$ $e^2 = 4Q'^2/3\pi^2$, we have

$$f(r) = 1 - \frac{8M}{3\pi r^2} - \frac{4Q'^2}{3\pi r^4} + \frac{r^2}{l^2}, \tag{15}$$

$$T' = \frac{r_+}{\pi l^2} + \frac{1}{2\pi r_+} - \frac{2Q'^2}{3\pi^2 r_+^5}, \tag{16}$$

$$S' = \frac{\pi^2}{2}r_+^3. \tag{17}$$

In this case, the solution reduces to the five-dimensional Reissner–Nordström AdS black hole. The phase transition of the Reissner–Nordström AdS black hole has been discussed extensively [13,28]. The critical values of the phase transition are given as

$$S_C{}' = \frac{\pi^2}{6\sqrt{3}}l^3, \tag{18}$$

$$Q_C{}' = \frac{\pi}{6\sqrt{5}}l^2, \tag{19}$$

$$T_C{}' = \frac{4\sqrt{3}}{5\pi l}. \tag{20}$$

Here, we mainly focus on studying the phase structure for the case $q \neq 0$.

Now, we begin to explore the hairy black hole's critical behavior and phase transition in the temperature–entropy plane. From Eqs. (13) and (14), we can get the function $T(S, Q, q)$ by eliminating r_+,

$$\begin{aligned} T(S,Q,q) =& \frac{1}{3\sqrt[3]{2}l^2\pi^{5/3}(5\pi^2 q + 4S)^{5/3}}\Big[75\pi^4 q^2 \\ & -128l^2\pi^2Q^2 + 120\pi^2 Sq + 48S^2 \\ & +9\sqrt[3]{4}l^2\pi^{10/3}q(5\pi^2 q + 4S)^{1/3} \\ & +6\sqrt[3]{4}l^2\pi^{4/3}S(5\pi^2 q + 4S)^{1/3}\Big]. \end{aligned} \tag{21}$$

Note that the phase structure of a hairy black hole is not only related to electric charge Q, but also the scalar hair parameter q. Based on the function $T(S, Q, q)$ above, the phase structure of the charged hairy black hole can be detected. We find that, by choosing some proper hair parameters q, the isocharges in the T–S plane can exhibit a Van der Waals-like phase transition. For convenience, we keep the AdS radius $l = 1$ throughout this paper. Here, we discuss the phase transition in a fixed electric charged ensemble, and we take

Table 1 The critical values of the electric charge, temperature and entropy for different q

q	Q_C	T_C	S_C
−0.010	0.0486384	0.439591	1.03476
−0.005	0.0538006	0.440337	0.992571
0.005	0.0629513	0.441770	0.906233
0.010	0.0670977	0.442460	0.862219

$q = \pm 0.010$ and $q = \pm 0.005$ as examples. To plot the isocharges in the T–S plane, firstly we should get the critical values of phase transition by using the following relations:

$$\left(\frac{\partial T}{\partial S}\right)_Q = \left(\frac{\partial^2 T}{\partial^2 S}\right)_Q = 0. \tag{22}$$

For the complicated hairy black hole, it is hard to obtain analytical values directly. We can get them numerically. In Table 1, we tabulate the critical charge Q_C, critical entropy S_C and critical temperature T_C for different hair parameter q. From this table, we see that the critical entropy becomes smaller as q increases. According to Eq. (14), we know that q must satisfy $q \leqslant 2r_+^3/5$ in order for the positivity condition of entropy to hold.

Note that, for the very small values of the hair parameter, one can get a perturbative solution of the critical values. When q is very small, we expand Eq. (21) about the zero point in terms of the hair parameter q, and we find

$$\begin{aligned} & T(S,Q,q) \\ &= \frac{-32\pi^2Q^2 + 32^{1/3}\pi^{4/3}S^{4/3} + \frac{12S^2}{l^2}}{62^{2/3}\pi^{5/3}S^{5/3}} \\ &\quad + \frac{\pi^{1/3}\left(30S^2 + l^2(400\pi^2Q^2 - 32^{1/3}\pi^{4/3}S^{4/3})\right)q}{362^{2/3}l^2S^{8/3}} \\ &\quad - \frac{5\left(\pi^{7/3}(1600l^2\pi^2Q^2 + 32^{1/3}l^2\pi^{4/3}S^{4/3} + 30S^2)\right)q^2}{432(2^{2/3}l^2S^{11/3})} \\ &\quad + O[q]^3. \end{aligned} \tag{23}$$

This corresponds to

$$T = \left(-\frac{e^2}{2\pi r_+^5} + \frac{1}{2\pi r_+} + \frac{r_+}{l^2\pi}\right) + \frac{q}{4\pi r_+^4} + O[q]^2. \tag{24}$$

When $q = 0$ and $e^2 = 4Q'^2/3\pi^2$, the temperature becomes the temperature of the RN AdS black hole, which is consistent with Eq. (16). Employing Eqs. (22) and (23), we can get

$$S_C = \frac{l^3\pi^2}{6\sqrt{3}} - \frac{7\pi^2 q}{8} + O[q]^2, \tag{25}$$

$$|e_C| = \frac{8}{\sqrt{3}}\left(\frac{l^2\pi}{24\sqrt{5}} + \frac{3\sqrt{\frac{3}{5}}\pi q}{8l}\right) + O[q]^2, \tag{26}$$

$$T_C = \frac{4\sqrt{3}}{5l\pi} + \frac{9q}{20l^4\pi} + O[q]^2. \tag{27}$$

When $q = 0$ and $e^2 = 4Q'^2/3\pi^2$, these questions reduce to Eqs. (18), (19) and (20). Obviously, for these small values, these critical quantities are modified from the RN AdS values.

According to the relation in Eq. (21) and these critical values, we plot the isocharges in the T–S plane for different q in Fig. 1. Each curve corresponds to a different electric charge. Remarkably, as can be seen from these plots, a Van der Waals-like phase transition is clearly present in the T–S plane. For different q, the phase structure is similar. When $Q > Q_C$, the temperature is monotonically larger as entropy increases, and the system is thermodynamically stable. As Q decreases and arrives at the critical value Q_C, an inflection point appears and the heat capacity is divergent at this point, which corresponds to a second order phase transition. In the $Q < Q_C$ case, in addition to two stable branches, the isocharge has an unstable branch with negative heat capacity,

$$C_Q = T\left(\frac{\partial S}{\partial T}\right)_Q, \tag{28}$$

which corresponds to a first order phase transition.

Like the Van der Waals phase transition of the liquid–gas system, this unstable portion should be replaced by using an isotherm $T = T^*$ which obeys Maxwell's equal-area prescription. The subcritical temperature T^* can be obtained from the plot of the free energy $F = M - TS$ versus the temperature. The plots in Fig. 2 show that the relations between the temperature and free energy for different q, and for $Q < Q_C$, we always observe a classic swallowtail structure in each plot, which is responsible for the first order phase transition in Fig. 1. We indicate the transition temperature T^* by a red dashed line in Fig. 2, which corresponds to the horizontal coordinate of the junction.

Next, in order to further characterize the Van der Waals-like phase transition, we turn to checking the Maxwell equal-area law for the first order phase transition and the corresponding statement can be written as

$$A_1 \equiv \int_{S_{\min}}^{S_{\max}} T(S,\ Q,\ q)\,\mathrm{d}S = T^*(S_{\max} - S_{\min}) \equiv A_2, \tag{29}$$

where $T(S,\ Q,\ q)$ is defined in Eq. (21), $S_{\min}$ and $S_{\max}$ are the smallest and largest roots of the equation $T(S,\ Q,\ q) = T^*$. Now, we take $q = -0.010$ as an example to show how to verify the Maxwell equal-area law. Numerically, using $q = -0.010$, $Q = 0.0286384$ and $l = 1$, we obtain T^* from the plot (a) in Fig. 2. Then, substituting $T^* = 0.4506$ into Eq. (21), we obtain the smallest value $S_{\min} = 0.306264$ and largest value $S_{\max} = 2.628909$ by resolving the equation $T(S, -0.01, 0.0286384) = 0.4506$. Thus,using the values of T^*, $S_{\min}$ and $S_{\max}$, we can get $A_2 = 1.04658$ at the right side of Eq. (29), and we obtain $A_1 = 1.04538$ by integrating the left side of Eq. (29). Namely, A_1 equals A_2 within our

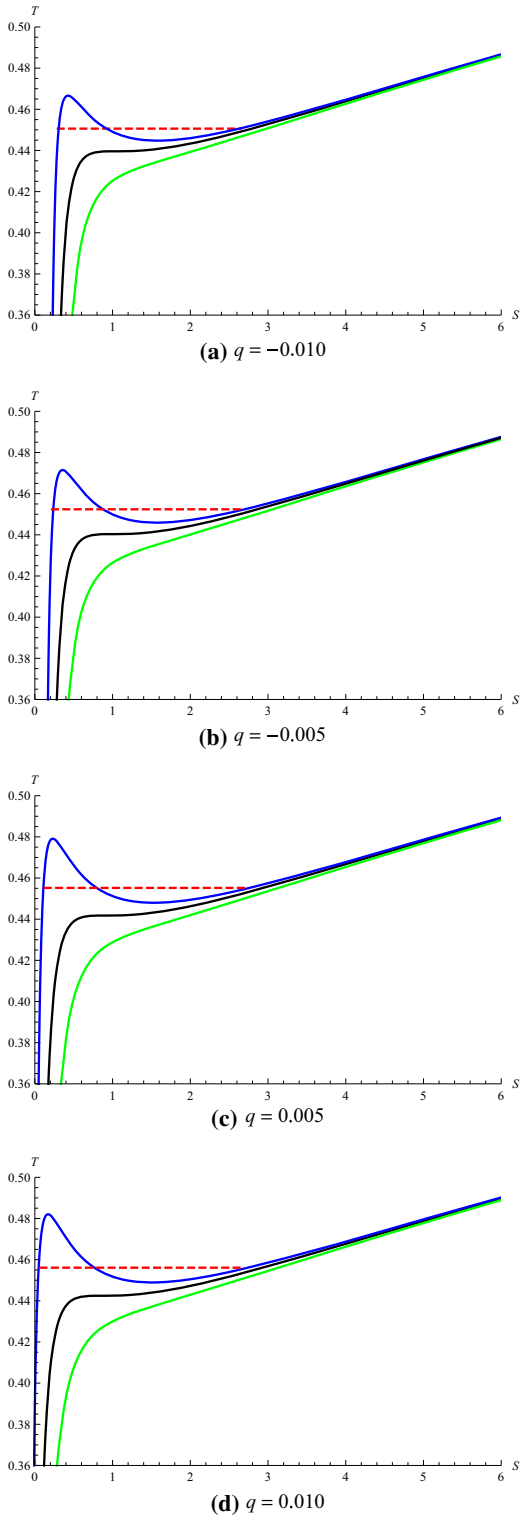

(a) $q = -0.010$

(b) $q = -0.005$

(c) $q = 0.005$

(d) $q = 0.010$

Fig. 1 Plots of the temperature versus the black hole entropy for different q. The red dash line corresponds to the temperature of the first order phase transition. The values of the electric charge chosen (from top to bottom) are as follows. **a** $Q = 0.0286384 < Q_C$, $Q = 0.0486384 = Q_C$, $Q = 0.0686384 > Q_C$. **b** $Q = 0.0338006 < Q_C$, $Q = 0.0538006 = Q_C$, $Q = 0.0738006 > Q_C$. **c** $Q = 0.0429513 < Q_C$, $Q = 0.0629513 = Q_C$, $Q = 0.0829513 > Q_C$. **d** $Q = 0.0470977 < Q_C$, $Q = 0.0670977 = Q_C$, $Q = 0.0870977 > Q_C$

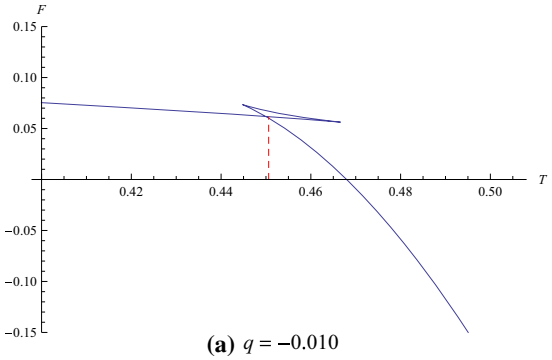

(a) $q = -0.010$

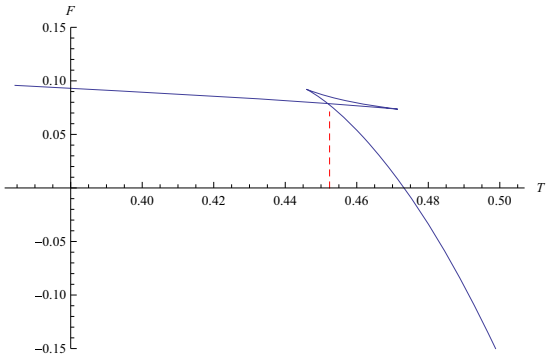

(b) $q = -0.005$

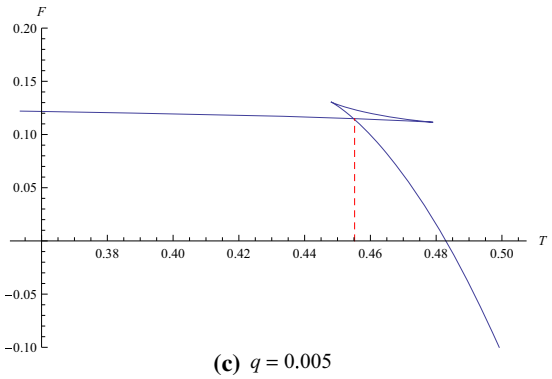

(c) $q = 0.005$

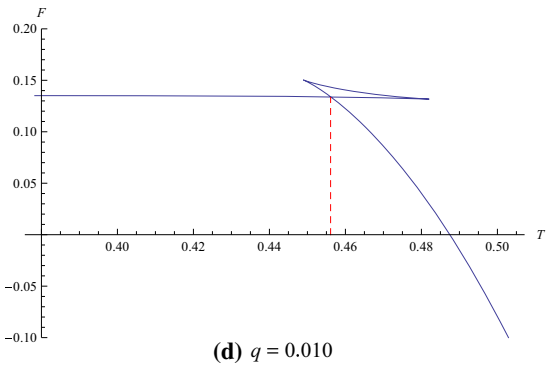

(d) $q = 0.010$

Fig. 2 Plots of the temperature versus the free energy for different q in the case of $Q < Q_C$. In each graph, the red dash line indicates a first order phase transition temperature T^*. **a** $Q = 0.0286384$ and $T^* = 0.4506$. **b** $Q = 0.0338006$ and $T^* = 0.4524$. **c** $Q = 0.0429513$ and $T^* = 0.4552$. **d** $Q = 0.0470977$ and $T^* = 0.4561$

Table 2 Check of the Maxwell equal-area construction in the T–S plane

q	T^*	$S_{\min}$	$S_{\max}$	A_1	A_2
−0.010	0.4506	0.3062640	2.6289090	1.04538	1.04658
−0.005	0.4524	0.2371192	2.6989999	1.11250	1.11375
0.005	0.4552	0.1098390	2.7624530	1.20665	1.20747
0.010	0.4561	0.0488927	0.7663060	1.22943	1.22924

numeric accuracy with these values. Repeating the procedure above, we can obtain A_1 and A_2 for other q, and we tabulate these values in Table 2. From this table, it is obvious that the Maxwell equal-area construction holds in the T–S plane.

3 Phase transition and Maxwell's equal-area law for two-point correlation function

In this section, we proceed to discuss on the phase structure of two-point correlation function. In recent years, the two-point correlation function has appeared to be a useful tool which can be used to explore some physical phenomena such as holographic singularities [29,30], holographic thermalization [31,32], holographic CFTs on maximally symmetric spaces [33], holographic butterfly effect [34–37] and quantum phase transition [38]. Motivated by the above-mentioned issues, we attempt to detect whether the two-point correlation function can present a Van der Waals-like behavior for the charged hairy black hole.

According to the Anti-de Sitter space/Conformal Field Theory dictionary, in the large $\triangle$ limit, the equal-time two-point correlation function can be holographically expressed as [39]

$$\left\langle O(t_0, x_i)\, O(t_0, x_j)\right\rangle \approx e^{-\triangle L}, \tag{30}$$

where $\triangle$ is the conformal dimension of the scalar operator O, and L is the length of the buck geodesic between the point $(t_0,\ x_i)$ and $(t_0,\ x_j)$ on the Anti-de Sitter boundary. Due to the charged hairy black hole's symmetry in five-dimensional AdS spacetime, we can simply set $(\theta = \theta_0,\ \varphi = \pi/2,\ \psi = 0)$ and $(\theta = \theta_0,\ \varphi = \pi/2,\ \psi = \pi)$ as the two boundary points.

By utilizing θ to parameterize the trajectory, the proper length takes the form

$$L = \int_0^{\theta_0} \mathcal{L}(r(\theta), \theta)\, \mathrm{d}\theta, \quad \mathcal{L} = \sqrt{\frac{r'^2(\theta)}{g(r)} + r^2(\theta)}; \tag{31}$$

here $r' \equiv \mathrm{d}r/\mathrm{d}\theta$. Taking $\mathcal{L}$ as the Lagrangian and imagining θ as time, with the Euler–Lagrange equation

$$\frac{\partial \mathcal{L}}{\partial r} = \frac{\mathrm{d}}{\mathrm{d}\theta}\left(\frac{\partial \mathcal{L}}{\partial r'(\theta)}\right), \tag{32}$$

we arrive at the equation of motion of $r(\theta)$,

$$g'(r)r'(\theta)^2 - 2g(r)r''(\theta) + 2g^2(r)r(\theta) = 0 \tag{33}$$

with the boundary condition

$$r(0) = r_0, \qquad r'(0) = 0. \tag{34}$$

By using the condition above and resolving Eq. (33), we obtain the numeric result of $r(\theta)$. Notice that the geodesic length is divergent for a fixed θ_0, therefore, it needs to be regularized. Here, we do it by subtracting the geodesic length of the minimal surface in pure AdS with the same boundary $\theta = \theta_0$ (denoted by L'). In order to accomplish this, we first obtain L by integrating the length function in Eq. (31) from zero to UV cutoff $\theta_C \lesssim \theta_0$. Then, by turning off the hair parameter q, mass M and electric charge Q of the charged hairy black hole background, we get a pure AdS in global coordinates,

$$\mathrm{d}s^2 = -\left(1 + \frac{r^2}{l^2}\right)\mathrm{d}t^2 + \left(1 + \frac{r^2}{l^2}\right)^{-1}\mathrm{d}r^2 + r^2\mathrm{d}\Omega_3^2, \tag{35}$$

with this metric, repeating the same procedure as calculation L, numerically, we obtain L'. Thus, subtracting this quantity from the hairy black hole, we get the renormalized geodesic length $\delta L = L - L'$. Here, we take $\theta_0 = 0.45$ and $\theta_0 = 0.50$ as an example to discuss the charged hairy black hole's phase structure, and the corresponding cutoffs are chosen to be $\theta_C = 0.449$ and 0.499 in the numerical computations. For the $\theta_0 = 0.45$ case, in Fig. 3, we present the plots of the isocharges generated for the two-point correlation function for different hair parameters q. In each panel, the isocharges in the T–δL plane from top to bottom correspond to $Q < Q_C$, $Q = Q_C$ and $Q > Q_C$, respectively. From these plots, we see that the T versus δL plots are qualitatively similar to the ones in Fig. 1. We confirm that there exists indeed a Van der Waals-like phase transition in the T–δL plane, and the critical temperature and critical charge are the same as the ones obtained from Fig. 1.

In order to further characterize a Van der Waals-like phase transition for the two-point correlation function, we choose two different θ_0 to verify the equal-area law in the T–δL plane, similarly defined as

$$\begin{aligned} A_1 &\equiv \int_{\delta L_{\min}}^{\delta L_{\max}} T(\delta L,\, q,\, Q)\,\mathrm{d}\delta L \\ &= T^*(\delta L_{\max} - \delta L_{\min}) \equiv A_2, \end{aligned} \tag{36}$$

where $\delta L_{\min}$ and $\delta L_{\max}$ are the smallest and largest roots of the equation $T(\delta L,\, q,\, Q) = T^*$. $T(\delta L,\, q,\, Q)$ is an interpolating function which can be given by our numeric result.

Besides $\theta_0 = 0.45$, in Fig. 4, for the case $\theta_0 = 0.50$, we also plot the isocharge in the T–δL plane when the charge

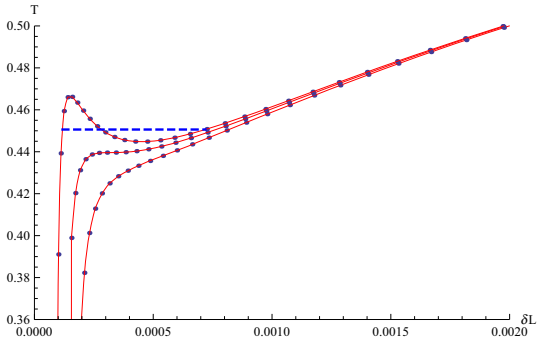

(a) $q = -0.010$

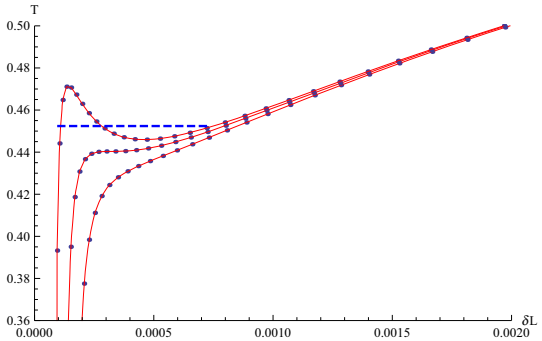

(b) $q = -0.005$

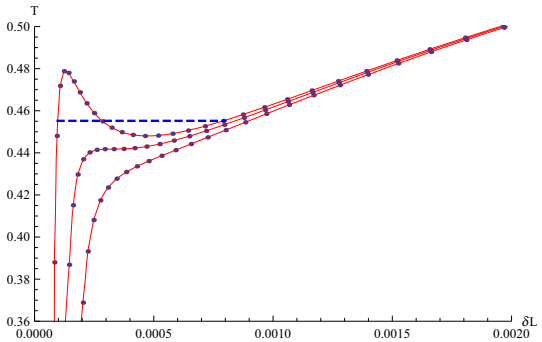

(c) $q = 0.005$

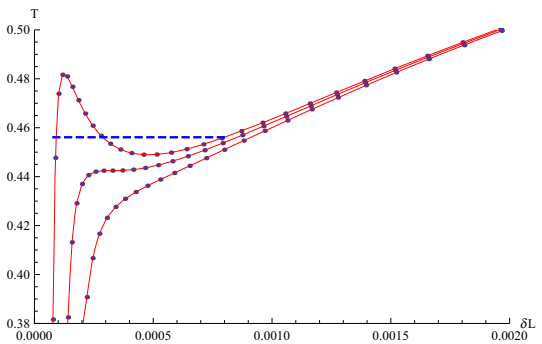

(d) $q = 0.010$

Fig. 3 Plots of isocharges in the T–δL plane for $\theta_0 = 0.45$. The blue dash line corresponds to the temperature of the first order phase transition. The values of the electric charge chosen (from top to bottom) are the same as the ones in Fig. 1

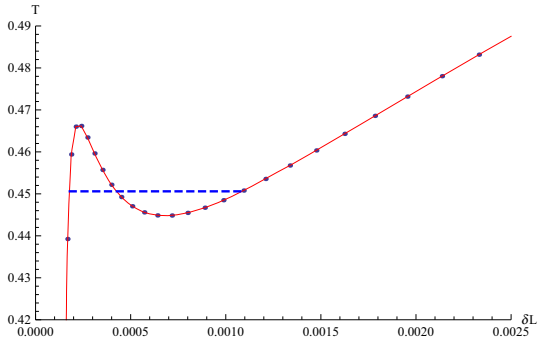

(a) $q = -0.010$

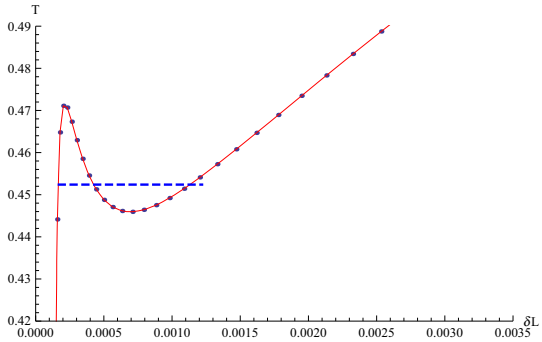

(b) $q = -0.005$

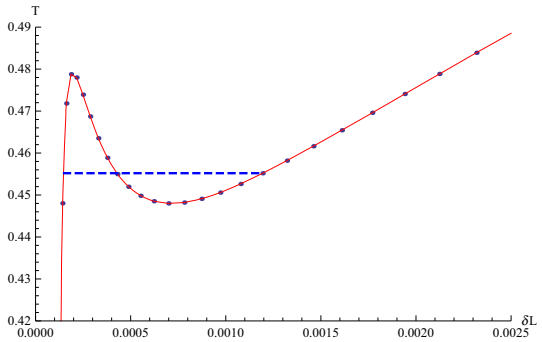

(c) $q = 0.005$

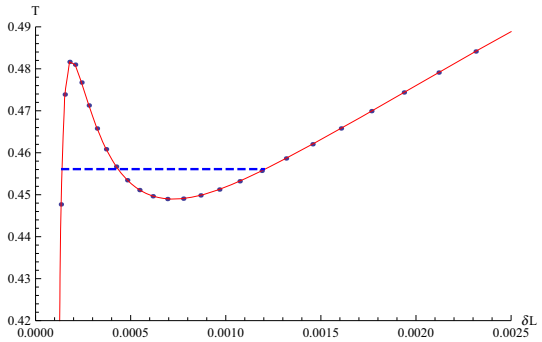

(d) $q = 0.010$

Fig. 4 Plots of isocharges in the T–δL plane for $\theta_0 = 0.50$. The blue dash line corresponds to the temperature of the first order phase transition for $Q < Q_C$. **a** $Q = 0.0286384 < Q_C$. **b** $Q = 0.0338006 < Q_C$. **c** $Q = 0.0429513 < Q_C$. **d** $Q = 0.0470977 < Q_C$

Table 3 Check of the Maxwell equal-area construction in the T–δL plane

		$\theta_0 = 0.45$		$\theta_0 = 0.50$	
$q = -0.010$	$T^* = 0.4506$	$\delta L_{\min} = 0.0001181430$	$A_1 = 0.00027069$	$\delta L_{\min} = 0.0001788345$	$A_1 = 0.00040808$
		$\delta L_{\max} = 0.0007194292$	$A_2 = 0.00027094$	$\delta L_{\max} = 0.0010853080$	$A_2 = 0.00040846$
$q = -0.005$	$T^* = 0.4524$	$\delta L_{\min} = 0.0001099755$	$A_1 = 0.00028904$	$\delta L_{\min} = 0.0001664403$	$A_1 = 0.00043580$
		$\delta L_{\max} = 0.0007494337$	$A_2 = 0.00028929$	$\delta L_{\max} = 0.0011305550$	$A_2 = 0.00043617$
$q = 0.005$	$T^* = 0.4552$	$\delta L_{\min} = 0.00009738140$	$A_1 = 0.00031608$	$\delta L_{\min} = 0.0001473907$	$A_1 = 0.00047660$
		$\delta L_{\max} = 0.00079196240$	$A_2 = 0.00031617$	$\delta L_{\max} = 0.0011947060$	$A_2 = 0.00047674$
$q = 0.010$	$T^* = 0.4561$	$\delta L_{\min} = 0.00009229728$	$A_1 = 0.00032276$	$\delta L_{\min} = 0.0001397911$	$A_1 = 0.00048686$
		$\delta L_{\max} = 0.00079951970$	$A_2 = 0.00032256$	$\delta L_{\max} = 0.0012065893$	$A_2 = 0.00048657$

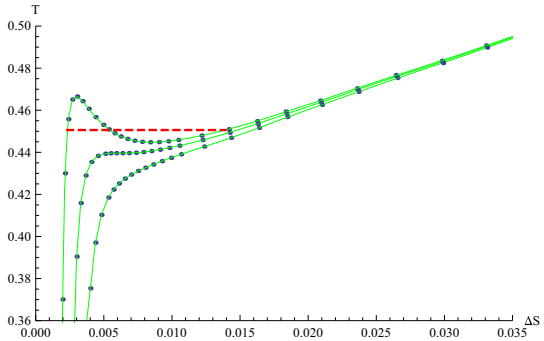

(a) $q = -0.010$

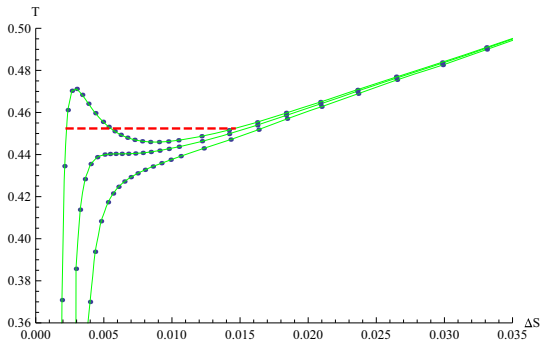

(b) $q = -0.005$

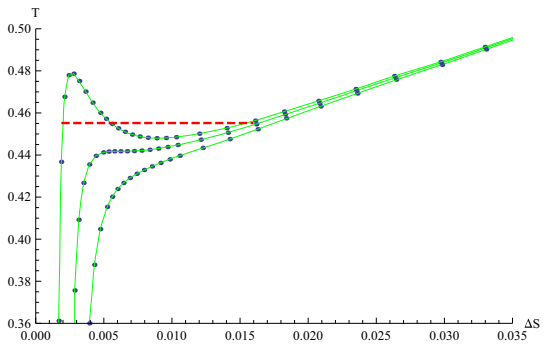

(c) $q = 0.005$

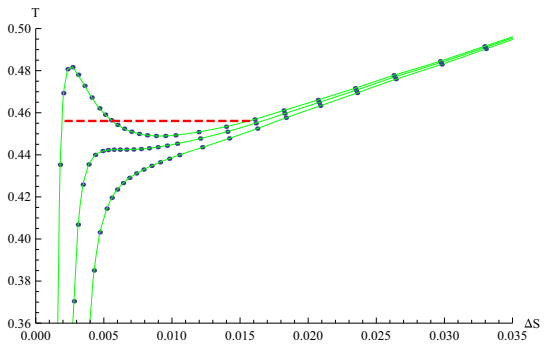

(d) $q = 0.010$

Fig. 5 Plots of isocharges in the T–$\triangle S$ plane for $\varphi_0 = 0.45$. The red dash line corresponds to the temperature of the first order phase transition. The values of the electric charge chosen (from top to bottom) are the same as the ones in Fig. 1

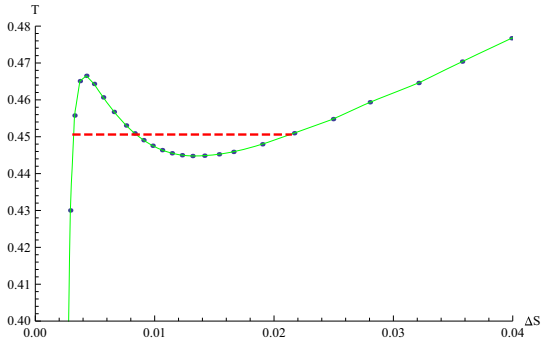

(a) $q = -0.010$

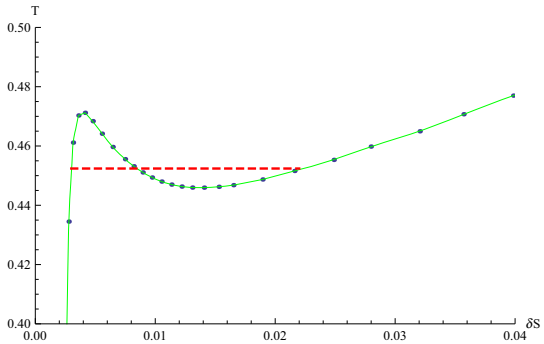

(b) $q = -0.005$

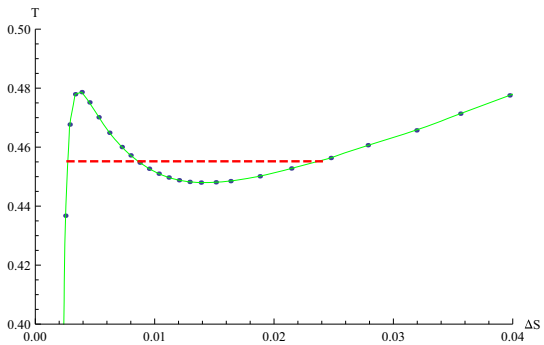

(c) $q = 0.005$

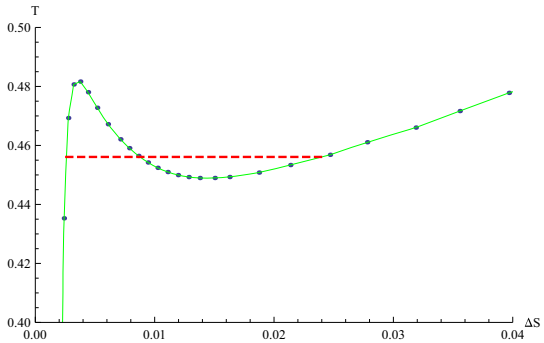

(d) $q = 0.010$

Fig. 6 Plots of isocharges in the T–$\triangle S$ plane for $\varphi_0 = 0.50$. The red dash line corresponds to the temperature of the first order phase transition for $Q < Q_C$. **a** $Q = 0.0286384 < Q_C$. **b** $Q = 0.0338006 < Q_C$. **c** $Q = 0.0429513 < Q_C$. **d** $Q = 0.0470977 < Q_C$

satisfies $Q < Q_C$. In Table 3, for different q and θ_0, we tabulate the values of $\delta L_{\min}, \delta L_{\max}, A_1$ and A_2. Obviously, for the two-point correlation function, the equal-area law hods for the five-dimensional charged hairy black hole. This strengthens our conclusion that, indeed, the isocharges in the T–δL plane can present the same Van der Waals-like phase transition as the black hole entropy.

4 Holographic phase transition for entanglement entropy

Now, we move on to take into account the entanglement entropy case. According to the Ryu–Takayanagi description, the holographic entanglement entropy for a region A can be expressed as [40,41]

$$S = \frac{\text{Area}(\Gamma_A)}{4}, \tag{37}$$

where Γ_A is a codimension-2 minimal surface with boundary condition $\partial\Gamma_A = \partial A$. Here, we choose $\varphi = \varphi_0$ as the hairy black hole's entangling surface and employ $r(\varphi)$ to parameterize the minimal surface.

With the symmetry, in this static AdS background, the entanglement entropy is given by

$$S = \pi \int_0^{\varphi_0} r^2 \sin^2\varphi \sqrt{\frac{r'^2(\varphi)}{f(r)} + r^2(\varphi)}\, \mathrm{d}\varphi, \tag{38}$$

in which $r'(\varphi) \equiv \mathrm{d}r/\mathrm{d}\varphi$.

Adopting a similar procedure to the two-point correlation function case, we first arrive at the equation of motion of $r(\varphi)$ by utilizing the Euler–Lagrange equation, and with the boundary condition, the numerical result of $r(\varphi)$ is obtained. Then we integrate the entropy function S in Eq. (38) up to the UV cutoff φ_C (that is, $\varphi_C \approx \varphi_0$). Thus, subtracting the pure AdS entanglement entropy (which is denoted by S_0), we are able to get the regularized entanglement entropy $\triangle S = S - S_0$ of a charged hairy black hole.

Specifically, choosing $\varphi_0 = 0.45$, we present the isocharges in the T–$\triangle S$ plane for different hair parameters q in Fig. 5. Comparing with Figs. 1 and 3 again, we find that, like the black hole entropy and two-point correlation function, the entanglement entropy also exhibits a Van der Waals-like phase transition; moreover, the critical charge and critical temperature are also identified with them.

We go on to verify whether the Maxwell construction works for the entanglement entropy in the T–$\triangle S$ plane. The analogous equal-area law becomes

$$\begin{aligned} A_1 &\equiv \int_{\triangle S_{\min}}^{\triangle S_{\max}} T(\triangle S, q, Q)\, \mathrm{d}\triangle S \\ &= T^*(\triangle S_{\max} - \triangle S_{\min}) \equiv A_2, \end{aligned} \tag{39}$$

where $\triangle S_{\min}$ and $\triangle S_{\max}$ are the smallest and largest roots of $T(\triangle S, q, Q) = T^*$, $T(\triangle S, q, Q)$ is an interpolating function which is given by our numeric result, and T^* is a transition temperature, which is equal to the first order phase transition temperature T^* found for black hole entropy in Sect. 2. In order to verify the equal-area law, we take $\varphi_0 = 0.45$ and $\varphi_0 = 0.50$ as example, we also present the isocharges in the T–$\triangle S$ plane for $\varphi_0 = 0.50$ in Fig. 6. For different q and φ_0, the numeric results of $\triangle S_{\min}$, $\triangle S_{\max}$, A_1 and A_2 are listed in Table 4. According to this table, we conclude that the Maxwell equal-area construction in the T–$\triangle S$ plane is valid within a reasonable error. Again, the result shows that like the black hole entropy, the entanglement entropy can indeed present a Van der Waals-like phase transition for the charged hairy black hole.

5 Discussion and conclusion

Note that recent work has indicated that the equal-area law is only valid very near the critical point [42]. Here, for the equal-area law of the entanglement entropy and two-point correlation function, by employing the same equal-area law as that used in Ref. [42], we perform numerical computations to explore this problem with the different ratios $Q/Q_C = 0.9$ and 0.5. The relevant numerical results have been put in Tables 5, 6, 7 and 8. Here, the relative error is taken to be the difference between A (I) and A (II) divided by their average. From these tables, it is obvious that Maxwell equal-area law is only valid near the critical point. Away from the critical point, the relative error becomes significantly large, and the Maxwell equal-area law cannot hold on these planes, which supports the point in the light of [42]. As far as the entanglement entropy and the two-point correlation function are concerned, a holographic equal-area law is still an open question.

In this paper, in the framework of holography, we discuss the phase structure of a charged hairy black hole in five-dimensional AdS background (in the fixed electric charge ensemble). The result shows that a Van der Waals-like phase transition can be observed in the T–S plane, T–δL plane and T–$\triangle S$ plane, and the critical charge and critical temperature are equal. Notice that, for some q value, where the gravity background exhibits a negative entropy, there no longer exists a reasonable phase transition. In order to guarantee that the entropy is positive, the scalar hair parameter q must satisfy the condition $q \leqslant 2r_+^3/5$. Since the corresponding expression for the critical values are too complicated in this charged hairy AdS background, here, we proceed to compute numerically.

It is interesting to note that, for the charged hairy black hole, in Ref. [7], Hennigar and Mann have first revealed a reentrant phase transition, and they have carefully studied

Table 4 Check of the Maxwell equal-area construction in the T–$\triangle S$ plane

		$\varphi_0 = 0.45$		$\varphi_0 = 0.50$	
$q = -0.010$	$T^* = 0.4506$	$\triangle S_{\min} = 0.002343243$	$A_1 = 0.0052170$	$\triangle S_{\min} = 0.00321284$	$A_1 = 0.0081764$
		$\triangle S_{\max} = 0.013932195$	$A_2 = 0.0052220$	$\triangle S_{\max} = 0.02136945$	$A_2 = 0.0081814$
$q = -0.005$	$T^* = 0.4524$	$\triangle S_{\min} = 0.00227335$	$A_1 = 0.0055859$	$\triangle S_{\min} = 0.00302369$	$A_1 = 0.0087256$
		$\triangle S_{\max} = 0.01463187$	$A_2 = 0.0055910$	$\triangle S_{\max} = 0.02232081$	$A_2 = 0.0087300$
$q = 0.005$	$T^* = 0.4552$	$\triangle S_{\min} = 0.00201383$	$A_1 = 0.0061112$	$\triangle S_{\min} = 0.00273341$	$A_1 = 0.0095445$
		$\triangle S_{\max} = 0.01544459$	$A_2 = 0.0061137$	$\triangle S_{\max} = 0.02369990$	$A_2 = 0.0095440$
$q = 0.010$	$T^* = 0.4561$	$\triangle S_{\min} = 0.00193166$	$A_1 = 0.0062515$	$\triangle S_{\min} = 0.00261655$	$A_1 = 0.0097623$
		$\triangle S_{\max} = 0.01563169$	$A_2 = 0.0062486$	$\triangle S_{\max} = 0.02400015$	$A_2 = 0.0097531$

Table 5 Check of the Maxwell's area law in the T–δL plane for $q = 0.010$ and $\theta_0 = 0.45$

T^*	Q	Q/Q_c	A (I)	A (II)	Relative error
0.447060	0.0603879	0.9	2.42670×10^{-7}	2.61054×10^{-7}	0.0182480
0.464856	0.0335489	0.5	9.12172×10^{-6}	6.55055×10^{-6}	0.0820291

Table 6 Check of the Maxwell equal-area law in the T–δL plane for $q = -0.010$ and $\theta_0 = 0.50$

T^*	Q	Q/Q_c	A(I)	A (II)	Relative error
0.442300	0.0437746	0.9	1.24830×10^{-7}	1.35112×10^{-7}	0.0197772
0.451123	0.0243192	0.5	3.55393×10^{-6}	2.44831×10^{-6}	0.0921010

Table 7 Check of the Maxwell equal-area law in the T–$\triangle S$ plane for $q = -0.010$ and $\varphi_0 = 0.45$

T^*	Q	Q/Q_c	A (I)	A (II)	Relative error
0.442300	0.0437746	0.9	1.54531×10^{-6}	1.70203×10^{-6}	0.0241305
0.451123	0.0243192	0.5	4.50689×10^{-5}	3.12496×10^{-5}	0.0905374

Table 8 Check of the Maxwell equal-area law in the T–$\triangle S$ plane for $q = 0.010$ and $\varphi_0 = 0.50$

T^*	Q	Q/Q_c	A (I)	A (II)	Relative error
0.447060	0.0603879	0.9	8.04075×10^{-6}	7.81503×10^{-6}	0.00711788
0.464856	0.0335489	0.5	2.73991×10^{-4}	1.93884×10^{-4}	0.08560700

the criticality and the Van der Waals behavior in the P–V plane. Here, in the T–S plane, by choosing some proper values of q, we also present the Van der Waals-like phase transition, thereby strengthening the conclusion of Ref. [7]. It is worth emphasizing that, motivated by holography, besides the black hole entropy, we also make use of the two-point correlation function and entanglement entropy to detect the Van der Waals-like phase transition.

Acknowledgements We thank the anonymous reviewers for careful reading of our manuscript and their many insightful comments and suggestions. We would like to thank Xiao-Xiong Zeng for his helpful discussions. This work is supported by the National Natural Science Foundation of China (Grant nos. 11573022 and 11703018).

References

1. J.M. Maldacena, Adv. Theor. Math. Phys. **2**, 231 (1998)
2. S.W. Hawking, D.N. Page, Commun. Math. Phys. **87**, 577 (1983)
3. A. Chamblin, R. Emparan, C.V. Johnson, R.C. Myers, Phys. Rev. D **60**, 104026 (1999)
4. A. Chamblin, R. Emparan, C.V. Johnson, R.C. Myers, Phys. Rev. D **60**, 064018 (1999)
5. D. Kastor, S. Ray, J. Traschen, Class. Quantum Grav. **26**, 195011 (2009)
6. A.M. Frassino, D. Kubiznak, R.B. Mann, F. Simovic, JHEP **1409**, 080 (2014)
7. R.A. Hennigar, R.B. Mann, Entropy **17**, 8056 (2015)
8. S.W. Wei, Y.X. Liu, Phys. Rev. D **91**, 044018 (2015)
9. S.H. Hendi, A. Sheykhi, S. Panahiyan, B. Eslam Panah, Phys. Rev. D **92**, 064028 (2015)

10. T. Delsate, R. Mann, JHEP **1502**, 070 (2015)
11. C.V. Johnson, JHEP **1403**, 047 (2014)
12. E. Caceres, P.H. Nguyen, J.F. Pedraza, JHEP **1509**, 184 (2015)
13. P.H. Nguyen, JHEP **1512**, 139 (2015)
14. X.X. Zeng, H. Zhang, L.F. Li, Phys. Lett. B **756**, 170 (2016)
15. X.X. Zeng, X.M. Liu, L.F. Li, Eur. Phys. J. C **76**, 616 (2016)
16. X.X. Zeng, L.F. Li, Phys. Lett. B **764**, 100 (2017)
17. X.X. Zeng, Y.W. Han. arXiv:1706.02024 [hep-th]
18. S. He, L.F. Li, X.X. Zeng, Nucl. Phys. B **915**, 243 (2017)
19. M.V. Bebronne, P.G. Tinyakov, JHEP **0904**, 100 (2009)
20. D. Comelli, F. Nesti, L. Pilo, Phys. Rev. D **83**, 084042 (2011)
21. J. Oliva, S. Ray, Class. Quant. Grav. **29**, 205008 (2012)
22. N. Bocharova, K. Bronikov, V. Melnikov, Vestn. Mosk. Univ. Fiz. Astronom. **6**, 706 (1970)
23. D. Bekenstein, Ann. Phys. **82**, 535 (1974)
24. G. Giribet, M. Leoni, J. Oliva, S. Ray, Phys. Rev. D **89**, 085040 (2014)
25. M. Galante, G. Giribet, A. Goya, J. Oliva, Phys. Rev. D **92**, 104039 (2015)
26. G. Giribet, A. Goya, J. Oliva, Phys. Rev. D **91**, 045031(2015)
27. R.A. Hennigar, R.B. Mann, E. Tjoa, Phys. Rev. Lett. **118**, 021301 (2017)
28. X.X. Zeng, L.F. Li, Adv. High Energy Phys. **2016**, 6153435 (2016)
29. N. Engelhardt, T. Hertog, G.T. Horowitz, JHEP **1507**, 044 (2015)
30. N. Engelhardt, T. Hertog, G.T. Horowitz, Phys. Rev. Lett. **113**, 121602 (2014)
31. X.X. Zeng, B.W. Liu, Phys. Lett. B **726**, 481 (2013)
32. X.X. Zeng, X.M. Liu, B.W. Liu, JHEP **03**, 031 (2014)
33. K. Hinterbichler, J. Stokes, M. Trodden, Phys. Rev. D **92**, 065025 (2015)
34. S.H. Shenker, D. Stanford, JHEP **1403**, 067 (2014)
35. S. Leichenauer, Phys. Rev. D **90**, 046009 (2014)
36. N. Sircar, J. Sonnenschein, W. Tangarife, JHEP **1605**, 091 (2016)
37. R.G. Cai, X.X. Zeng, H.Q. Zhang. arXiv:1704.03989 [hep-th]
38. J.G. Russo, M. Tierz, Phys. Rev. D **95**, 031901 (2017)
39. V. Balasubramanian, S.F. Ross, Phys. Rev. D **61**, 044007 (2000)
40. S. Ryu, T. Takayanagi, Phys. Rev. Lett. **96**, 181602 (2006)
41. S. Ryu, T. Takayanagi, JHEP **0608**, 045 (2006)
42. F. McCarthy, D. Kubiznak, R.B. Mann. arXiv:1708.07982 [hep-th]